Scientific Research Publishing

Engineering, 2025, 17(10), 529-553
https://www.scirp.org/journal/eng
ISSN Online: 1947-394X
ISSN Print: 1947-3931

Testing Oil-Brine and Polymer-Silica IFT with Pendant Drop (Rising Bubble) Method

Fahad Rashid*, Godpower Enyi

Petroleum and Gas Engineering Division, School of Science, Engineering, and Environment, University of Salford, Manchester, UK
Email: *rashidfahad314@gmail.com

How to cite this paper: Rashid, F. and Enyi, G. (2025) Testing Oil-Brine and Polymer-Silica IFT with Pendant Drop (Rising Bubble) Method. *Engineering*, **17**, 529-553.
https://doi.org/10.4236/eng.2025.1710030

Received: September 21, 2025
Accepted: October 27, 2025
Published: October 30, 2025

Abstract

This paper examines how polymer-coated nanoparticles (PNPs) affect interfacial tension (IFT) and their possible use in oil recovery (EOR). In particular, the paper investigates how the IFT between brine and dead oil can be lowered with the help of PNPs prepared with Arabic gum and silica nanoparticles at different temperatures and salinity. IFT was measured at pressures of 25 to 1900 psi and temperatures varying between 25˚C and 55˚C using the pendant drop technique. They demonstrate a continuous decline of IFT with temperature (the highest observed one is at 55˚C). Furthermore, elevated salinity (NaCl) resulted in reduced IFT, but it resulted more at high concentrations. High IFT further was reduced by the presence of silica nanoparticles and Arabic gum with the largest IFT reduction of about 46% potentially occurring in the brine-oil system with nanoparticles. These results indicate that PNPs may provide an attractive solution to enhancing EOR due to their ability to lower IFT, improve the efficiency of oil displacement transport in more difficult reservoirs. The research prepares the ground of additional studies regarding the use of nanotechnology in EOR processes.

Keywords

Enhanced Oil Recovery, Interfacial Tension, Polymer-Coated Nanoparticles, Silica Nanoparticles, Gum Arabic, Brine, Temperature, Salinity, Pendant Drop Method, Oil Displacement

1. Introduction

With the global economy increasingly becoming large, the consumption of energy (and oil in particular) is also rising. According to the International Energy Agency (IEA), the world will need 30% more energy in 2040 than in 2022, and oil will still be in the center of global demand. But the number of new oil discoveries is shrink-

ing, and the secondary and primary methods of extracting conventional oil can recover only a small portion of the oil within a single oil field. Primary recovery systems can usually only retrieve 10% of the oil, whereas secondary ones, involving the use of water or gas to aid recovery odds, can potentially extract an extra 30% - 40% [1]. Oil left behind, often stranded in the reservoir either through high viscosity or ineffective displacement, creates major potential for tertiary oil recovery or enhanced oil recovery (EOR) techniques.

The improvement of oil production in a reservoir past current capabilities with traditional methods has led to the development of EOR techniques, including chemical flooding. Chemical flooding uses chemicals to decrease IFT between water and oil, enhancing the displacement and sweep of injected fluids. These agents reduce the IFT, enabling more oil to be displaced and recovered in the reservoir. This technique has the potential to improve the recovery rate by between 10% - 20% over conventional techniques [2].

Nanotechnology has emerged as the latest method to enhance EOR practices. Nanoparticles have a size of between 1 and 100 nanometers and provide multiple benefits, such as a higher surface area, greater reactivity, and better interaction with oil and reservoir rock [3]. Nanotechnology has exhibited potential in enhancing chemical flooding processes, recovering oil and gas, and in the utilisation of surfactants and polymers among other chemical agents.

Nonetheless, as nanoparticles have proven to be effective in EOR, the use of polymer-coated nanoparticles (PNPs) is an emerging development. Through the attachment of polymer chains onto nanoparticles, PNPs exhibit increased stability, solubility, and mobility in reservoirs. Its polymer coating enhances the preservation of emulsions and foams, which are typically essential to enhancing displacement efficiency during chemical flooding [4]. Another important aspect is that the polymer coating improves the mobility of the nanoparticles through the porous medium, which means that the nanoparticle delivery can be used to access the targeted zones in the oil reservoir and optimise recovery.

This study will specifically focus on investigating the behavior of polymer gum Arabic-covered silica nanoparticles with brine at different temperatures to determine how effective they will be in suppressing IFT and increasing oil displacement. The Gum Arabic is chosen as it is a naturally occurring polymer that is well known to be active in aqueous environments and has potential uses as an oil recovery agent. Silica nanoparticles are selected since they have compatibility with both oil and water and thus are good candidates in applications involving chemical flooding strategies. Its purpose is not to provide an extensive literature review, but to consider how these new materials-polymer-coated nanoparticles can surmount the constraints of the traditional EOR methods and enhance oil recovery even in challenging reservoir environments. Through examination of the IFT reduction by PNPs, the study will evaluate their ability to enhance oil recovery particularly in poorly controlled reservoirs of conventional chemical flooding compounds.

Gum Arabic (GA) offers several advantages over synthetic polymers commonly used in EOR, such as polyacrylamides. It is a natural, biodegradable, and non-toxic polysaccharide with strong emulsifying and stabilizing properties, which enables it to improve nanoparticle dispersion and stability even under high-salinity conditions [5]. Compared with petroleum-derived polymers, GA is more environmentally sustainable and cost-effective, while also enhancing interfacial adsorption due to its amphiphilic molecular structure. Silica nanoparticles (SiO_2), on the other hand, are amphiphilic, inexpensive, and possess tunable surface chemistry that allows strong anchoring at the oil-water interface, leading to significant IFT reduction and wettability alteration [6]. When combined, GA and SiO_2 provide a synergistic effect: GA prevents nanoparticle aggregation and enhances colloidal stability, while silica reinforces the interfacial film formed by GA, producing a more robust barrier to droplet coalescence. This synergy distinguishes the GA-SiO_2 system from conventional polymer-nanoparticle formulations, positioning it as a novel and environmentally friendly approach for EOR applications [7].

The goal of this work is to help create more efficient, cost-effective, and scaled-up methods of EOR, potentially increasing oil recovery levels by 15% - 20% or more. The work, it is hoped, will lead to a fuller utilisation of nanotechnology in the oil and gas industry, so to ensure that the world has an adequate supply of oil and energy to meet its growing demand. The main interest of the work is the exploration of the potential of polymer-coated nanoparticles (PNPs) to limit the interfacial tension (IFT) of oil reservoirs, thereby enhancing oil recovery (EOR). Since energy needs globally are expanding, the need to boost oil reserves within the same reservoirs becomes highly significant, especially when there is a decline in new oil fields. Whereas primary and secondary oil recovery methods have been actively employed, they can extract only a portion of oil in reservoirs. EOR, also known as tertiary recovery processes, can be used to recover oil that would otherwise not be produced. The current work is aimed at evaluating how PNPs, including those based on polymer gum Arabic and silica nanoparticles, can be used to enhance the recovery process by lowering IFT and enhancing the overall efficiency of oil displacement.

2. Introducing the Interfacial Tension Theory

Within the process of calculating the interfacial tension of the air bubble, the form of the bubble is taken into consideration. The use of a radius of curvature (R_i) and the shape effect (β) involves the utilisation of Equations (1) and (2) to accomplish this.

$$\gamma = \Delta\rho g\left(\frac{R_i^2}{\beta}\right) \tag{1}$$

And

$$\Delta\rho = \rho_{\text{gas phase}} - \rho_{\text{liquid phas}} \tag{2}$$

In this equation, the word $\Delta\rho$ is used to describe the magnitude of the disparity in density that exists amid the persistent bubble phase and the larger bubble phase.

Regarding the drooping bubble, the variable g represents the gravitational constant, β is the structural element, and R_i is the radius of curvature at the bubble's apex. Equations (3)-(5) shows how the Young-Laplace calculation, expressed in a dimensionless manner, has been used to define the bubble contour.

$$\frac{\mathrm{d}\theta}{\mathrm{d}S} = 2 - \beta Y - \frac{\sin\theta}{X} \tag{3}$$

$$\frac{\mathrm{d}x}{\mathrm{d}S} = \cos\theta \tag{4}$$

$$\frac{\mathrm{d}x}{\mathrm{d}S} = \sin\theta \tag{5}$$

where X, Y and S are dimensionless quantity drive by dividing x, y and s with R_i as presented in Equation (6)-(8).

$$X = \frac{X}{R_i} \tag{6}$$

$$Y = \frac{y}{R_i} \tag{7}$$

$$S = \frac{s}{R_i} \tag{8}$$

The parameter denotes the coldness along the drop profile measured from the drop apex. The two distances, H'' and H', are measured from the apex of the drop to the midpoint of the curve depicting the fall. Many academic dimensionless profiles were generated throughout the whole feasible β-range, which included values ranging from $\beta = -0.55$ to 1020. This was achieved by Kutta-Merson's geometric addition method, which included automated step length adjustment. 10^{-4} was determined to be the largest feasible relative inaccuracy that could be achieved. The mathematical measurements that were performed on each profile were carried out with the use of cubic interpolation. Using this method, curves were formed, which demonstrated a connection between the parameters β and R_i and the calculable parameters that were shown in Figure 1. Following the formation of these curves, the method of least squares was used throughout the process of fitting them using linear polynomials.

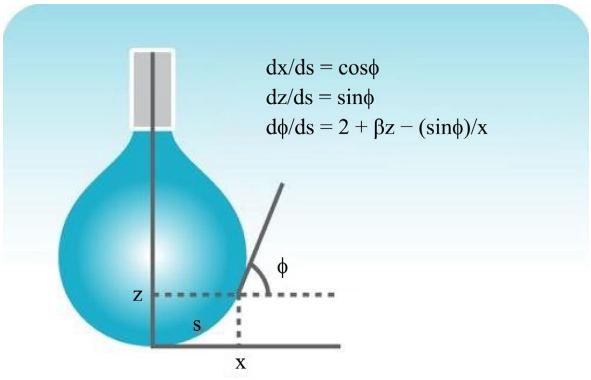

Figure 1. Showed the bubble with the images of the x, z, s and θ.

In situations where pendant drops are too short to determine DS the radius (R), the drop height (H), the three variables that are employed are the diameter at a distance D_E from the drop apex. Furthermore, the drop height is designated as the drop height. The expression for R in Equation (6) is as follows:

$$R = \frac{D_E}{2} \tag{9}$$

D_E is an abbreviation that stands for the greatest diameter of the methane gas bubble measured from its apex. It is possible to rewrite Equation (1) in terms of H, as shown in Equation (7), specifically as follows:

$$\gamma = \Delta\rho g\left(\frac{H}{\beta}\right)^2 \tag{10}$$

where $\Delta\rho$ is the difference in density between the bubble in the air and the liquid around it, g is the speed of sound due to gravity, R_i is the radius of curve at the drop's tip, and β is the shape factor. The $\Delta\rho$ is given by Equation (11):

$$\Delta\rho = \rho_{\text{air phase}} - \rho_{\text{liquid phase}} \tag{11}$$

The symbol β denotes a modified shape parameter. It is evident that H will possess a maximum value, since the surface tension can withstand the highest hydrostatic pressure, it is capable of enduring. The presumed limiting value of β is 2.0. When the droplet attains a state of infinite fullness, a single radius of curvature suffices for it to be deemed complete. Consequently, Equation (10) offers a far more effective approach for determining the dimensions of minuscule pendant bubbles. As can be seen in Equations (12) and (13), an additional parameter B may be determined as a purpose of the ratio $x = H/R$.

$$B = \beta * \left(\frac{H}{R_0}\right) = (X) \tag{12}$$

$$\frac{H}{R_0} = (X) \tag{13}$$

Combination calculation (12) and (13) yields (14):

$$b = (x)/g(x) \tag{14}$$

With these two functions, R_0 and β are easily determined for all values of β <1000 from the measurement of H and R and Equations (10) and (12).

3. Experiment

3.1. Oil

The crude oil from Kuwait has an API gravity of 22 degrees, which classifies it as medium crude. Table 1 presents a compilation of the characteristics of the crude oil.

Table 1. Oil sample is obtained from the University of Salford laboratory.

API	Viscosity	Density (g/m^3)	Classification
20.3	134.828	0.932	Medium oil

3.2. Arabic Gum Polymer

Acacia Senegal and Acacia Seyal trees are used to harvest the branches of the Acacia tree, which are then used to extract the Arabic gum. This is a dry, gummy exudate that may be consumed. Gum Arabic serves as a stabilising component, emulsifier, flavouring agent, thickening agent, and surface-finishing agent in the food industry owing to its considerable solubility properties. Furthermore, it inhibits the crystallisation of sugar or the onset of turbidity. In the wine production process, gum Arabic functions to inhibit dye colouring and protein precipitation.

3.3. Silica Nano Particles

Plastics, coverings, compound materials, rubber, and ceramics are just some of the types of applications that make use of this substance. Since it has a substantial hydrophilic property, it is suitable for oil systems (Table 2).

Table 2. Types of nanoparticles silica used in experimental.

Name	Appearance	Mean particle size	Purity	SSA
Processing of KH570 Nano Silicon dioxide powder	White powder	20 nm	99%	140.20 m^2/g

In accordance with the illustration in Figure 2, brine solution was used in conjunction with the mixture of silica nanoparticles and Arabic gum polymer. Brine is made by combining distilled water and sodium chloride, both of which are bought from Ajax. The salinity of the brine varies based on the sources that are extracted from the oilfield.

Figure 2. Mixing silica and AG with brine contained (5 wt%, 10 wt%, 15 wt% and 20 wt%).

4. Description of IFT Apparatus

4.1. Equipment and Concepts for Interfacial Tension

Experimental research on fluid phase relations has given rise to the development

of several tensiometers, which have become basic equipment in a range of technical processes. Of all the methodologies discussed, only a small number are currently common in measuring interfacial tension (IFT) at fluid liquid interfaces. [8] documented a short survey of the strategies that are currently considered to be the most frequent in measuring IFT, with a more comprehensive analysis. These researchers have made significant contributions in the science on interfacial tension measurement in that their work has contributed to a better insight into this experimental technique in exploring interfacial tension. The Pendant Drop (PD) method is one of the most common methods of measuring IFT at fluid-liquid interfaces due to its simplicity and versatility to study gas-liquid interfaces over an extended pressure and temperature scale [9]. It is regarded as the commonly used method to measure IFT in liquid phase systems. The PD method contains the production of a droplet of heavier fluid at the end of a capillary tube that is stabilised in the less dense surrounding fluids, whether liquid or vapor. This approach is intended to obtain the required density of droplets in the surrounding medium.

After the droplet is formed, the profile or the height of the liquid column is measured, and the morphology of the droplet is investigated. These measurements are subsequently added with phase density measurements to calculate the values of interfacial tensions. [10] stated that the PD approach was invented with the purpose of determining the effect of gravity on drop geometry, which directly impacts its profile. The main incentive behind the approach was to investigate the effect that gravity exerts on the appearance and dynamics of a drop that models a given volume of liquid. The discussion that follows is a brief historical and technical account of the theoretical underpinnings of these measurement techniques. In this section, we highlight the historical progression of measurement methods employed to measure IFT. Additionally, the device used in this research study to measure the interfacial tension of reservoir fluids in different experimental settings is also explained.

In this experimental design, the capillary, which is a calibrated tube, is mounted in a chamber, forming a fluid droplet. The resulting drop can be monitored by people attached to the computer system, as shown in **Figure 3**. The output is subsequently captured by the software built into the system, permitting rigorous analysis of the droplet morphology and, in the end, the interfacial tension. It can provide accurate manipulation of experimental conditions and will enable consistent measurement of IFT in a variety of fluid systems, which can be useful in the investigation of the fluid phase interactions in reservoir conditions.

Figure 3. Rising oil drop.

Modifications will be implemented to the settings for measuring IFT, as shown in Table 2. The first concentrations of the combination are formulated at weight percentages of 5%, 10%, 15% and 20%. There are a variety of salinity levels that are tried, including five weight percent, ten weight percent, fifteen weight percent, and twenty weight percent. It is then permitted for the temperature to vary between 25, 35, 45 and 55degrees Celsius. Finally, the pressure would be evaluated for their various values, which range from 25 to 1900 psi. Table 3 is a presentation of the operating settings that were used for this investigation.

Table 3. Operating parameters for the IFT measurement.

Parameters	Operating conditions
Combination (silica + GA)	0.55% and 0.50%
Salinity (%)	5%, 10%, 15% and 20%
Temperature (˚C)	25˚C, 35˚C, 45˚C and 55˚C

One of the most essential elements of the equipment was a piece of stainless steel that was formed like a cylinder. This device is equipped with a circular glass pane that allows for the observation and recording of the form of each rising bubble via the medium of photography and videography. The cell has a capacity of 39 cubic centimetres, and it is furnished with a circular glass window. Utilising the heating element that is positioned around the cell to control the temperature, as well as employing the chamber to control the temperature. To manufacture the needle, the insert hole, which is formed of stainless steel and is situated at the bottom of the cell, is used. To begin the procedure of measuring the interfacial tension, the first step was to fill the fluid sample cylinder with the fluid using either a manual pump or an automated pump. Alterations to the pressure that was contained inside the cylinder were accomplished using a manual pump in conjunction with a back pressure controller. The air supply linked to the capillary tube and the regulating valve are essential for effectively controlling the ascent of the appropriately sized bubble at the capillary tube's apex. For every shot in the collection, ten distinct metrics were applied. It was determined that the value of interfacial tension, that was regarded to be representative of the current inquiry was the average interfacial tension that was produced by the bubble profile at every agreed-upon experimental pressure and temperature.

4.2. Control of Vibration and Bubble Chamber

The bubble chamber is an important part of the system as it is the point of interaction between the liquid and gaseous samples where the interface forms. The system also contains a vibration control table and a measurement chamber as shown in Figure 4. The chamber is made of stainless steel, an ideal material because it can handle extreme humidity levels and pressures. With the ability to

withstand temperatures of up to 200˚C and pressures of up to 10,000 psi, the chamber is durable to withstanding the severe conditions during such experiments. The bottom end has a sealing port where needles are inserted, and a back-pressure controller is connected to an overflow valve at the top, which allows precise control of the pressure in the system. The inner volume of the chamber is 39 cubic centimeters. The chamber is connected to a vibrational control bench to keep it at the right orientation and reduce the errors in the measurement due to external vibrations. This bench is particularly optimised to minimise vibrations, thereby making the interfacial tension (IFT) measurements as accurate as possible. A combination of a robust chamber and vibration damping setup allows such a system to be usable within the stated experimental parameters

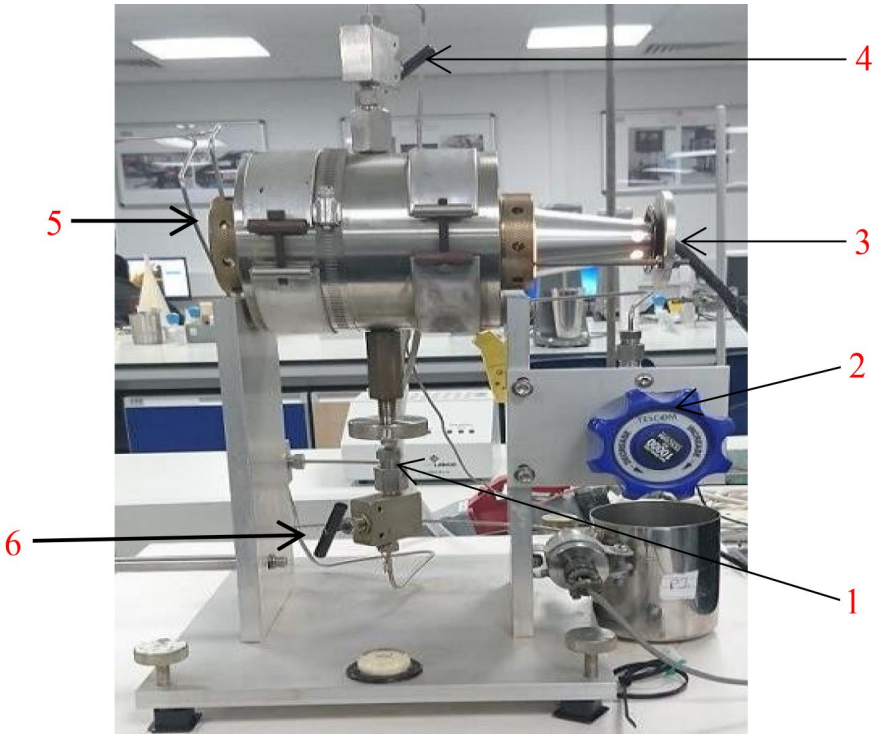

Figure 4. IFT-10 experiment exhibiting bubble chamber with various components (1-Injection Phase, 2-Back Pressure, 3-light source, 4-Upper Valve, and 5-Lowest Valve).

In line with the plan shown in **Figure 5**, the mounts of the bench companion are supplied with air via the use of a pump that is operated manually. It is necessary for the viewing glass to be situated at the front end of the chamber for the capturing camera to be able to take and record a live picture of the droplet or bubble. During this period, the light mate that is responsible for illumination is situated at the back of the cell. To light the fluid that is visible within the cell, which in turn makes it possible to observe the inside of the cell, its function is to illuminate the fluid. It is possible to establish a connection between the lower valve assembly and the capillary tube by using the bottom of the needle, which is attached to the lower valve assembly. This connection is accomplished by using the

needle. When the knurled stem is rotated, the needle tip is positioned in the right spot inside the cell for the generation of bubbles or drips. This is accomplished by turning the stem.

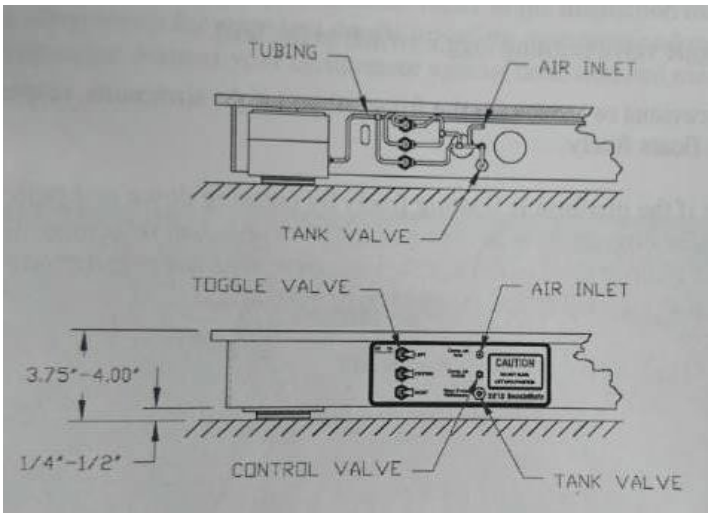

(a)

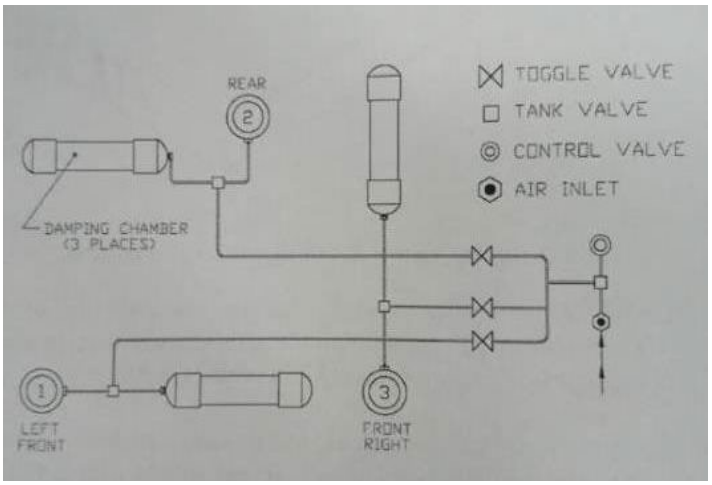

(b)

Figure 5. The control panel, air fill, and airline schematic in vibrational control schematic.

4.3. Automatic and Manual Pump

According to **Figure 6** a representation of both the automated and manual pumps that were used during the IFT measurement can be seen in the picture below. With the help of the Quizix Pump Works software, the QX-6000 automated pump is completely linked with the data collecting system and is being monitored in a continuous manner. This device is outfitted with a pump controller that is accountable for coordinating the activities of two separate positive displacement piston pumps, which are denoted by the letters A and B. When it comes to establishing a pulseless continuous fluid flow for a single fluid, it is conceivable for these two

piston pumps to operate independently for distinct stroke volumes. There is also the possibility that they will collaborate to provide a continuous flow of fluid for a single fluid. At this point, it is possible to make use of any of these pumps. With a stroke volume of around 12 centimetres cubic, a piston diameter of 0.375 inches, a maximum pressure of 6000 pounds per square inch, and a maximum flow rate of fifty cubic centimetres per minute, the device displays a range of capabilities. There are 0.375 inches of diameter on the piston. There is a possibility that the manual pump will help in elevating the cell's internal pressure.

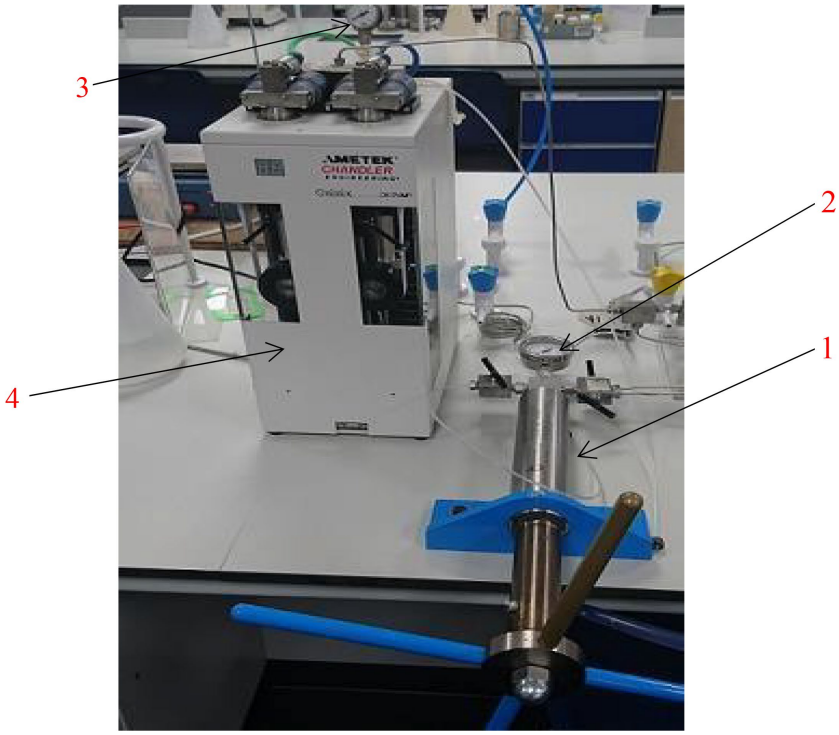

Figure 6. Section on manual and automated pumps (1-Manual Pump, 2-Pressure, 3-Compress Air Pressure, 4-Quizik Automatic).

4.4. The Rame-Hart Live-Image Camera

The Rame-hart digital video camera was placed outside the viewing chamber of the cell; A visual documentation of the droplet or bubble that formed inside the cell was obtained.

4.5. Data Acquisition System

A live feed was sent to the drop image software by the Rame-hart camera, which was connected to the personal computer. This allowed the program to do processing (**Figure 7**). There is a link between the suit and the Rame-hart camera, which is responsible for managing the transmission of the live image of the drop that is created in the cell for the purpose of additional analysis using the Advanced picture software to be performed. Using this connection, the suit is able to provide the picture.

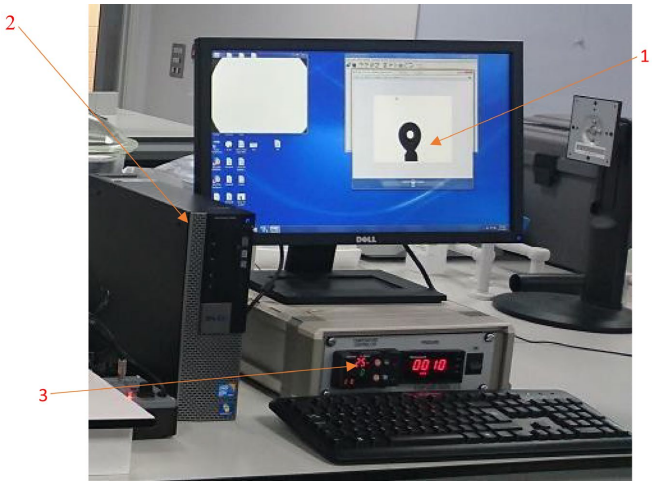

Figure 7. Section displaying data acquisition system (1-Window displaying drop image App, 2-CPU, 3-Temperature controller).

5. Experimental Procedures

One of the most important parts of the equipment was a piece of stainless steel that was cylindrical in shape. To make it easier to observe and record the configuration of every rising bubble, it is outfitted with a glass pane that is round. The cell features a square glass window and a capacity of 39 cubic centimetres. Additionally, the cell contains a circular glass window. The regulation of temperature is accomplished using a device known as a chamber, with the heating element being positioned all around the cell. At the very bottom of the cell is a hole of stainless steel that may be used for inserting. Utilisation of this aperture is intended to take place throughout the process of needle production. When it came to measuring interfacial tension, the first thing that needed to be done was to fill the fluid sample cylinder with fluid using either a human or an automated pump. It was necessary to carry out this technique to ensure accurate results. Both a manual pump and a back pressure regulator were used to maintain the desired level of pressure inside the cylinder. A valve is responsible for controlling the ascent of the bubble of the proper size that is situated at the very top of the capillary tube. A connection is made between the capillary tube and the air supply, and the valve is responsible for controlling the rising bubble. There were ten distinct metrics that were applied to each image in the collection. To achieve the goals of this investigation, the standard interfacial tension was calculated by making use of the values of interfacial tension that were obtained from the bubble profile at each of the experimental pressures and temperatures over the course of the investigation.

6. Steps of the Experimental Procedures

The pendent-drop system was shown in Figure 8 to be the most effective technique for regulating the interfacial tension (IFT) at the brine-crude oil interface. Within the context of this experimental setting, the procedure that was used included the production of a little oil droplet at the tip of a needle made of stainless

steel that was submerged in an aqueous brine composition. When this was taken into consideration, The experiments listed here were conducted:

1) To begin, insert a stainless-steel ball into an empty IFT cell to perform a calibration test.

2) To get the imaging equipment ready to capture a picture, it is being made ready.

3) Make the necessary adjustments to the horizontal/vertical apex ratio by selecting the calibration option and then running the program.

4) Take the ball out of the IFT cell and then proceed to adjust the location of the camera.

5) The IFT cell should be filled to its maximum capacity with synthetic brine.

6) In order to get consistent oil, drop on the top of the needle placed within the cell, it is necessary to carefully pump oil via the bottom needle.

7) A temperature control system should be used to set the temperature at the reservoir's value to achieve thermal stability inside the cell. The heating coats that are wrapped around the cell should be used.

8) When the brine is pumped into the cell, the pressure within the cell is increased to the same level as the reservoir pressure. Maintaining the oil drop on top of the bottom needle requires pumping oil simultaneously.

9) You should take photographs of the temperature and pressure in the reservoir.

10) To calculate IFT values, run the image drop image application.

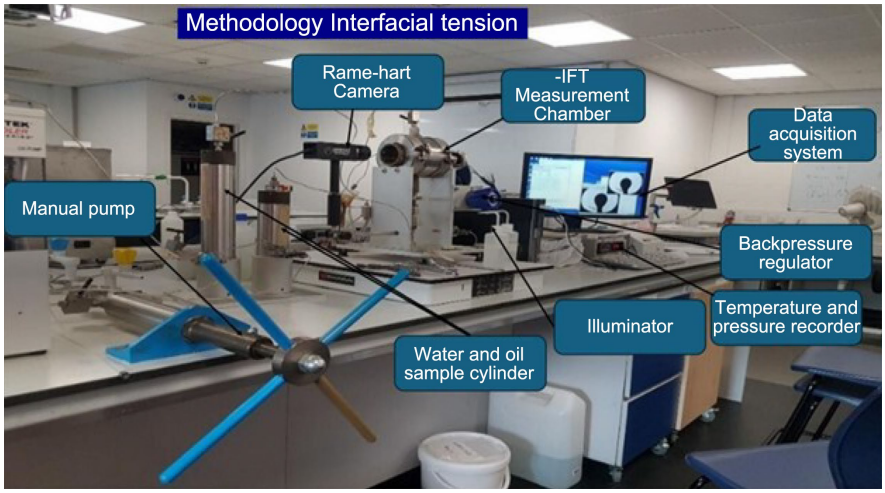

Figure 8. IFT (University of Salford) experimental setup and experimental setup.

To lessen the interfacial tension between oil and water, it is anticipated that the synthesis of Arabic gum and silica nanoparticles will proceed. The pendant drop technique is used to measure the original water-oil interfacial tension before the reduction of brine, silica, and Arabic gum. This occurs prior to the commencement of the reduction procedure. The pendant drop method relies on analysing the droplet shape formed when oil interacts with water, brine, or other fluids after

its passage through the needle. Upon examining the image below (Figure 9), one will see the pendant drop used for measuring interfacial tension.

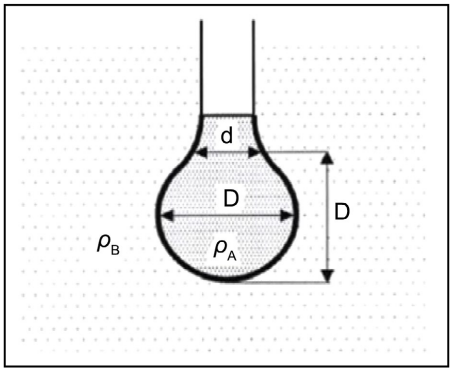

Figure 9. Dimensions and symbols used.

The objective of this procedure is to introduce an oil solution into a transparent cell by using a needle that is introduced into the bottom of the cell. Afterwards, the needle is used to inject oil into the cell after it has been filled with water or brine until it is about half full. This process is repeated until the cell is completely full. It is necessary to fill the cell with water or brine until it reaches the halfway point to make it possible to create an oil droplet. The interaction between the oil and the fluid that is coming out of the needle results in the formation of a droplet. Following that, a video camera is used to record this decrease. This cell is positioned in such a way that it will allow the camera to record the oil drop with precision. A computer loaded with drop analysis software is linked to a video camera that is attached to the computer. The apparatus that is used in the process of measuring interfacial tension is shown in the figure that can be seen below. An examination of many drops is carried out to get accurate measurements of the form of the drop. When the dimensions of the pendant drop are calculated, it is possible to determine the interfacial tension by this process. Additionally, the pendant drop approach may be used for the measurement of two different parameters. These parameters are the equatorial diameter, which is represented by the letter D, and the diameter, which is represented by the letter d about the base of the drop. Both parameters are included in the discussion. The exact position during the descent is the place from which both measurements are taken. Combining the two measurements results in what is known as the equatorial diameter. After the task has been completed, the equation that will be presented in the following paragraphs is used to calculate the interfacial tension.

$$\gamma = \frac{\Delta \rho g D^2}{H} \tag{15}$$

g = Gravity
D = Equatorial diameter
H = Shape parameter
ρ = Density

As shown in Figure 10, the IFT flowchart is a visual diagram that outlines a process or workflow in a clear, step-by-step manner.

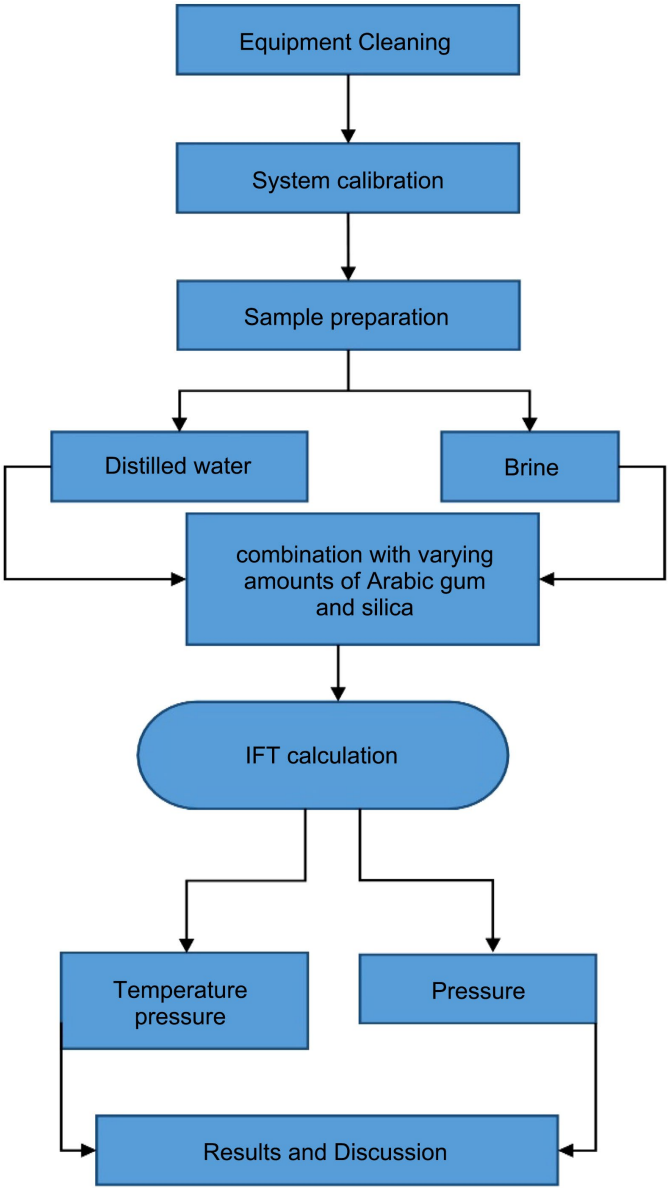

Figure 10. Experimental validation schematic.

7. Results and Discussion

7.1. Pressure and Temperature Influence on IFT

Figure 11 and Figure 12 display the findings of measurements that were taken of the interfacial tension (IFT) of bubbles of air in water. These measurements were conducted at a variety of temperatures and pressures. The pressure varies between 25 and 1900 psi, and the temperatures are 25, 35, 45 and 55, respectively. The IFT typically decreases as the levels of temperature and pressure rise. This kind of behaviour is a sign that, in a two-phase system that is comprised of water and air

and operating under typical pipeline conditions, the IFT drops as the pressure increases while the temperature is held at a constant level. In a similar vein, the IFT drops when temperature increases, even though pressure has a greater impact than temperature in this specific situation. This phenomenon is evidence that the surface of the water encounters an increase in the buildup of air molecules as the amount of pressure increases. As a result of the fact that they tend to connect with one another in water, this buildup of molecules makes it simpler for them to transmit over the contact. Furthermore, as the IFT falls, the transportation of air across the interface is enhanced.

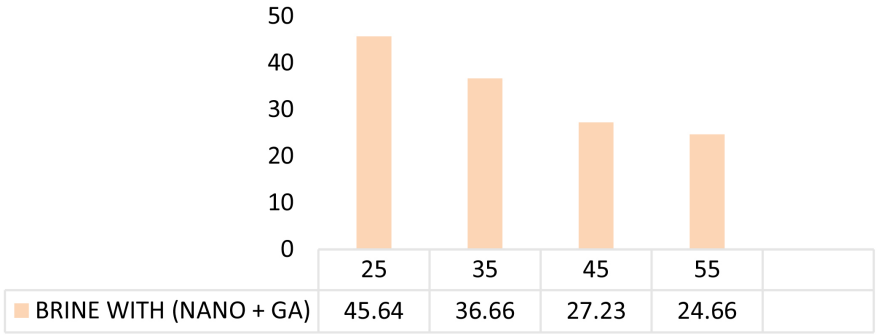

Figure 11. Effect of temperature on the IFT.

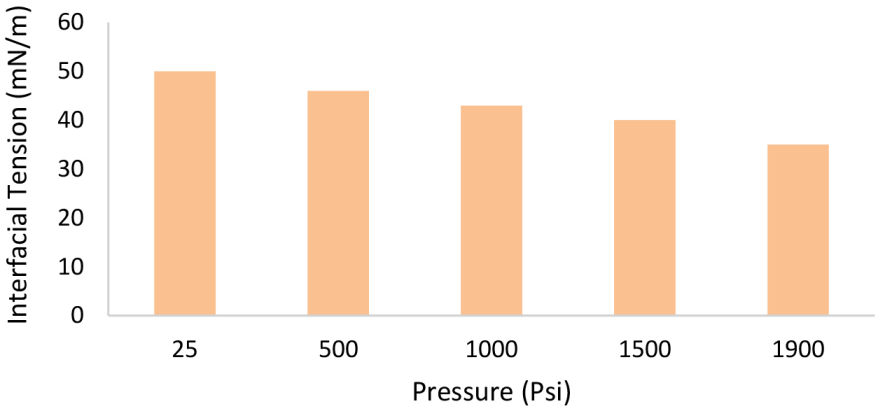

Figure 12. Effect of pressure on the IFT.

7.2. Air-Water Two-Phase System IFT

The interfacial tension (IFT) of air was determined by comparing the surface tension of air to that of distilled water, brine, and polymer-silica solutions. This was done to measure the quality of air. To create the brine solutions, several amounts of sodium chloride were used, namely 5, 10, 15, and 20 weight percent. Additionally, a variety of combinations of polymer and silica solutions that were mixed were put through their paces. The density of the aqueous solutions was also calculated and recorded, in addition to the IFT measurements that were taken. The findings are summarised in tabular form for the purpose of making comparisons and analyses more straightforward.

IFT for Air-Distilled Water

To ensure that the investigation was thorough and accurate, the IFT of the air-water system was compared to the information discovered in the literature. This was done to ensure that the study carried out the correct information. In addition, the results that were achieved by administering a variety of fluid solutions, including aqueous solutions, polymer fluids, silica fluids, and combination silica and polymer fluids, were also considered here. The purpose of this comparative research was to evaluate the impact that salts and fluid solutions have on IFT. This was the goal of the investigation. Furthermore, an investigation was undertaken to examine the impacts of system pressure and temperature by assessing interfacial tension across various pressure and temperature configurations. This experiment was carried out with the purpose of determining the degree to which these components influence the outcome. It is possible that the findings of this study will shed light on the behavioural patterns displayed by interfacial tension in a variety of fluid systems. This is something that is possible. The temperatures used in the experiments ranged from 25˚C to 55˚C, while the pressures used in the experiments ranged from 0 to 100 pounds per square inch. The effects of pressure and temperature were painstakingly studied and recorded in the report that was finally generated. This was done throughout the duration of the experiments.

There was 65.1 mN/m of interfacial tension (IFT) between air and distilled water 25˚C was 65.1 mN/m to 65.17 mN/m at 35˚C, then to 63.18 mN/m at 45˚C and 59.81 mN/m at 55˚C. It worked best when the temperature was between 25 and 55 degrees Celsius, where the interfacial tension dropped from 65.1 mN/m to 59.81 mN/m, which is a 8.12% drop as shown in Figure 13.

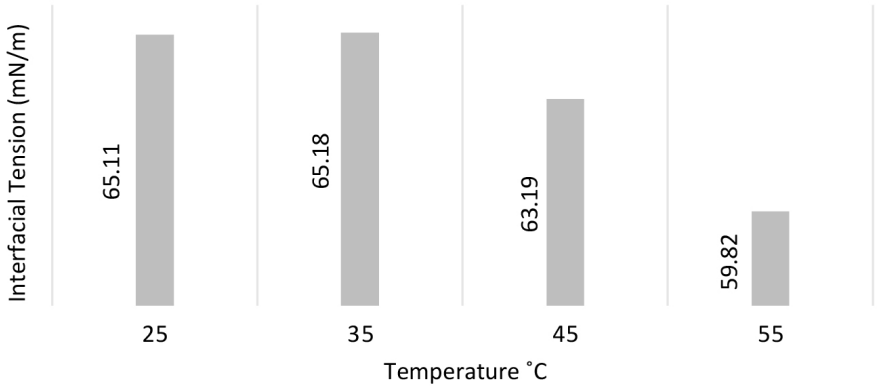

Figure 13. IFT: Distilled water-air at 25˚C, 35˚C, 45˚C, and 55˚C.

7.3. IFT Measurement between Fluid (Brine/Arabic Gum/Silica) and Air

7.3.1. Brine 5%

At 25˚C, the IFT between air and brine containing 5% was 21.47 mN/m; however, it dropped to 18.80 mN/m at 35˚C, and then it dropped to 15.44 mN/m and 9.65 mN/m at 45˚C and 55˚C, respectively. At 25˚C, the interfacial tension was 21.47 mN/m, which reduced to 9.65 mN/m at 55˚C, representing a reduction of about

55.05 percent (Figure 14).

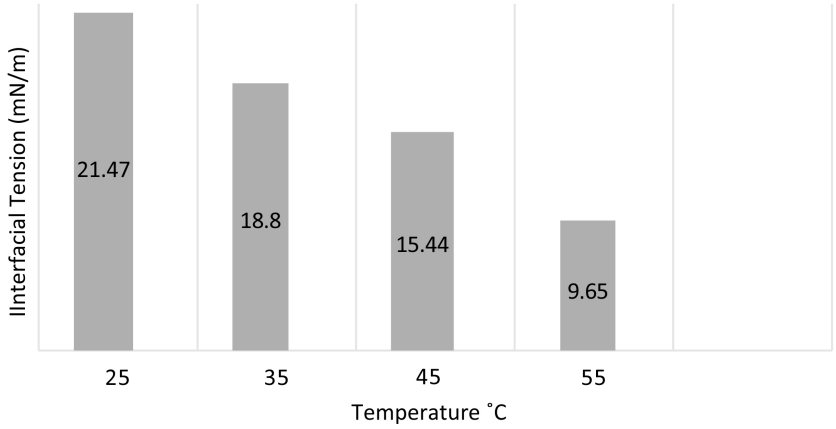

Figure 14. IFT-Brine 5%-air at 25˚C, 35˚C, 45˚C, and 55˚C.

7.3.2. Brine 10%

Using weight measurements, the interfacial tension (IFT) between air and a brine solution was determined at four distinct temperatures: 25˚C, 35˚C, 45˚C, and 55˚C. These temperatures were chosen since they all had different temperatures. 45˚C and 55˚C were the other temperatures that were recorded. The experiment was conducted with temperatures measured in degrees Celsius throughout its whole. Over the course of the experiment that was carried out, each one of these temperatures was used in their respective capacities. The initial IFT was measured to be 74.05 mN/m when the temperature was set at 25˚C. When the temperature reached 35˚C, the IFT dropped to 66.97 mN/m. After that, the IFT dropped even more to 61.68 mN/m at 45˚C, and then it dropped even further to 49.49 mN/m at 55˚C. Notably, the most substantial drop in IFT was recorded at the temperatures that were evaluated at the lowest and highest levels, which were 25 degrees Celsius and 55 degrees Celsius, respectively. As a result of these temperatures, the IFT dropped from 74.05 mN/m to 49.49 mN/m, which represents a decrease of around 33.61% (Figure 15).

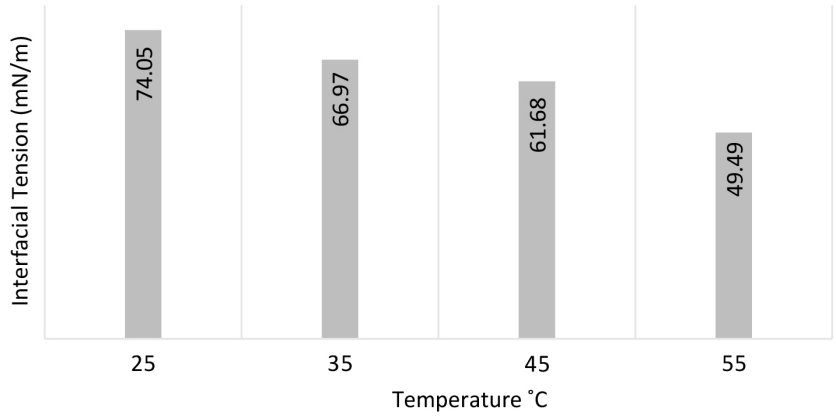

Figure 15. Brine 10% - air at 25˚C, 35˚C, 45˚C, and 55˚C.

7.3.3. Brine 15%

We investigated the interfacial tension (IFT) between air and a 15% brine solution at 25˚C, 35˚C, 45˚C, and 55˚C. At 25˚C, the initial interfacial tension was recorded as 17.54 mN/m. When the temperature was raised to 35˚C, the IFT began to rise to 13.26 mN/m. However, the IFT climbed to 12.17 mN/m when the temperature was 45˚C, but it decreased once more to 30.61 mN/m when the temperature was 55˚C (Figure 16).

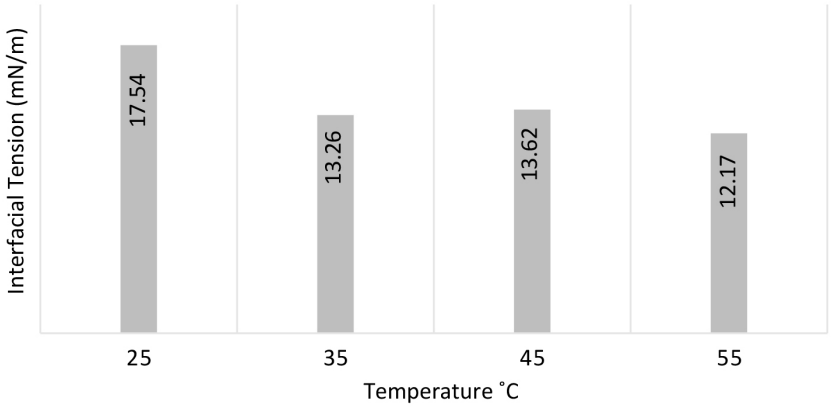

Figure 16. Brine 15% in air at 25˚C, 35˚C, 45˚C, and 55˚C.

7.3.4. Brine 20%

The IFT between air and brine at a concentration of 20 weight percent was tested at a variety of temperatures, and the findings indicate that the IFT dropped at warmer temperatures as well as at lower temperatures. At temperatures between 25˚C and 55˚C, the greatest results were achieved, with a drop in IFT of about 20.39 percent. It is essential to take notice of the fact that the IFT values are relatively low, which indicates that the system is conducive to the displacement of air and water (Figure 17).

Effect of NaCl concentration (5 - 20 wt%) on IFT between air and brine. Increasing salinity reduced IFT, though the trend plateaued at higher concentrations (Figure 18).

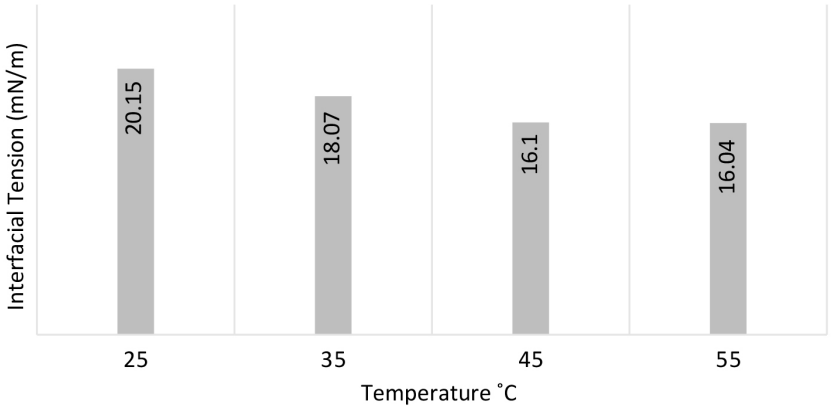

Figure 17. Brine 15% in air at 25˚C, 35˚C, 45˚C, and 55˚C.

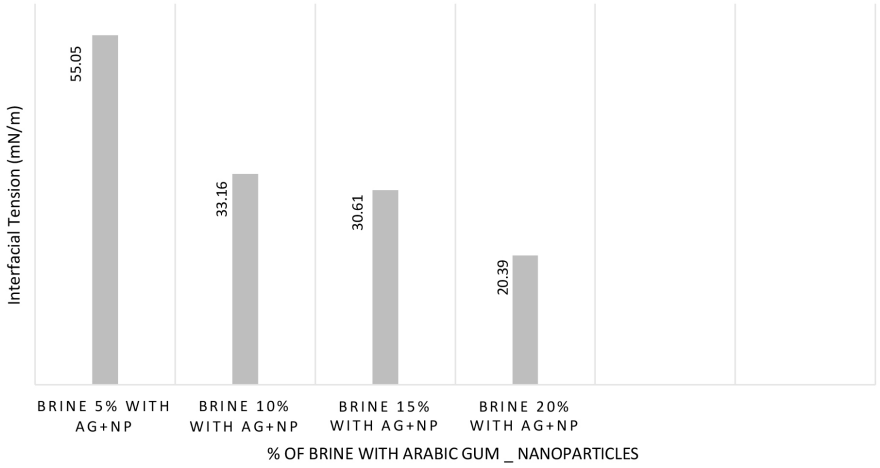

Figure 18. IFT between air and brine percentages at various temperatures.

7.4. Two-Phase Oil-Aqueous Solution (Silica-Polymer) IFT

IFT between Oil and Fluids

The pendant drop technique was shown to be the most efficient method for determining the interfacial tension (IFT) at different concentrations between fluids made of nanoparticles and crude oil. This was established by the findings of the study. To maintain a steady IFT value for the whole of this method, ambient circumstances were used. A decrease in the interfacial tension (IFT) that occurred between brine and crude oil was seen because of the existence of polymer Arabic gum and silica nanoparticles between the two substances, as shown by the results of the research. As the brine concentration increased, the IFT values between brine and crude oil were 19.23%, 18.57%, 15.47%, and 14.89%. The brine content showed a reduction from 19.23% to 14.89%, indicating that the brine content was decreasing. Figure 19 and Table 4 both illustrate the link that exists between the two unique kinds of liquids via their separate representations. For arriving at these values via the process of comparison, a comparison was conducted between the crude oil and the brine. Through the utilisation of 20% brine, a reduction of 14.89% was accomplished, while the utilisation of 15% brine resulted in a reduction of 15.47%, the utilisation of 10% brine resulted in a reduction of 18.57%, and the utilisation of 5% brine resulted in a reduction of 19.23%. All these reductions were accomplished by utilising brine.

Table 4. Summary of IFT values for air-brine and oil-brine systems with varying NaCl concentration and the addition of gum Arabic-silica nanoparticles. Elevated salinity and nanoparticles both reduced IFT, with the strongest reduction observed at 20 wt% brine with nanoparticles.

Aqueous	Distilled water	5 wt%	10 wt%	15 wt%	20 wt%	Brine with nano and GA
IFT	8.98%	19.22%	18.56%	15.46%	14.88%	46.0%

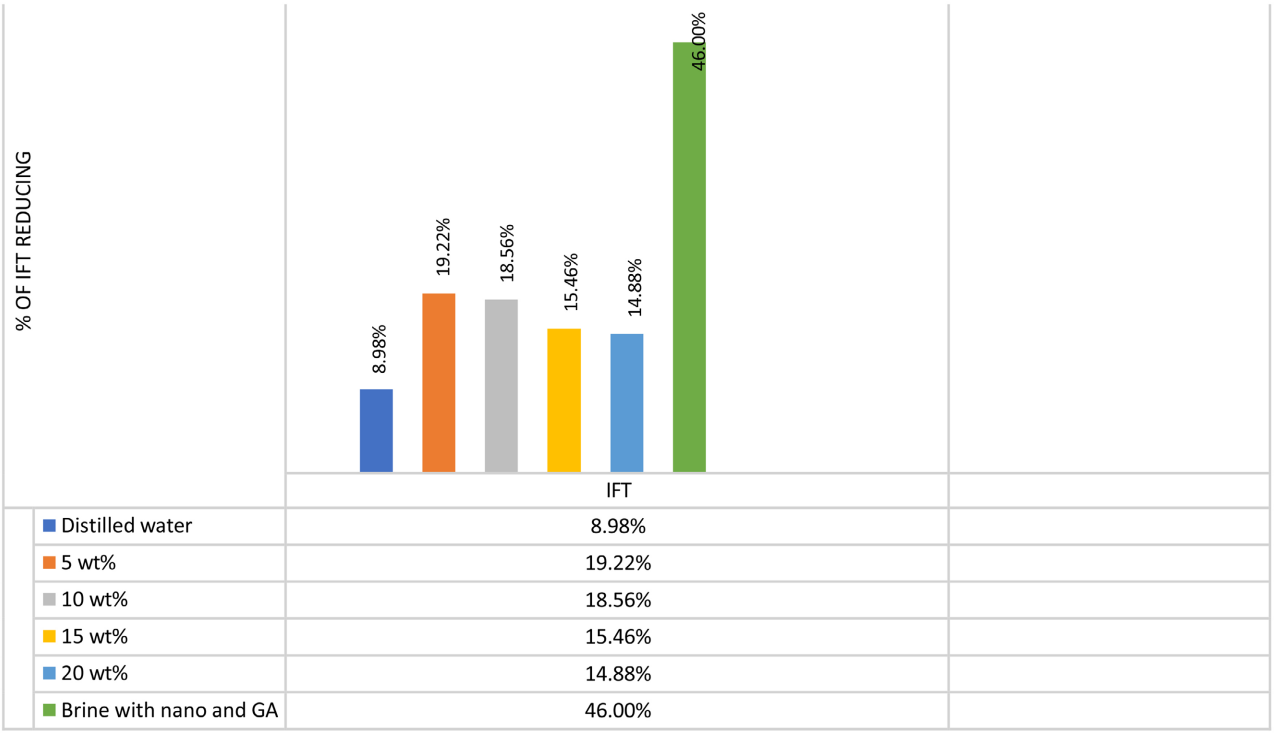

Figure 19. IFT of oil and brine percentages with silica and polymer at various temperatures.

Figure 19 depicts the outcomes of the experiments that were conducted using a combination of Arabic gum and silica nanoparticles in conjunction with brine at a concentration of 5%. A decrease in interfacial tension (IFT) was seen throughout a wide temperature range, as shown by the data. It was observed that there was a decrease in IFT that was about 46.01 hundred percent.

8. Discussion

8.1. Effect of Pressure on IFT

IFT measurements were conducted at pressures ranging from 25 to 1900 psi to evaluate the role of pressure in interfacial behavior. The results show a consistent trend of decreasing IFT with increasing pressure. At 25 psi, the IFT values were relatively higher, while at 1900 psi the IFT values were the lowest across all systems tested (air-brine, brine-oil, and nanoparticle-modified systems). This reduction in IFT with pressure is attributed to the compression of fluid phases at elevated pressures, which promotes stronger molecular interactions at the interface and reduces interfacial energy. Although the magnitude of the pressure effect was less significant than that of temperature, salinity, or nanoparticle addition, its influence was measurable and consistent across all test conditions.

The effect of pressure on IFT was also considered, with measurements performed between 25 and 1900 psi. The results confirmed that IFT decreases as pressure increases, in agreement with prior studies that reported reduced interfacial energy at higher pressures. This trend can be explained by the enhanced density

of the liquid phase under compression, which modifies the molecular arrangement at the fluid interface and decreases cohesive forces. Compared with the effects of temperature, salinity, and nanoparticles, the influence of pressure was smaller but still significant, suggesting that pressure should not be neglected when assessing reservoir conditions for enhanced oil recovery. In practical applications, the combined effects of elevated pressure and temperature may further improve the efficiency of IFT reduction when nanoparticles and biopolymers are employed.

8.2. Effects of Temperature on IFT

The reducing rate of IFT with elevation of temperature as observed in this study are in line with those of previous researchers. Literature reveals that the leading cause of this decline is the attenuation of intermolecular forces at the oil/brine/air/water interface caused by temperature rise. Since kinetic energy of molecules is elevated with increase of temperature, attraction between the molecules at the interface weakens which in turn causes a decrease in the IFT [11]. The occurrence of this trend has been recorded in much research on the nature of IFT in aqueous and oil-based systems. The reduction of IFT in the example of a brine-oil system might also be explained by the fact that the solubility of both surfactants and other types of additives is increased when the temperature is higher, and, thus, the interfacial tension is decreased further [12]. Such impact has been addressed concerning the concept of enhanced oil recovery (EOR), whereby temperature has been adopted to improve the utilisation of surfactants in the reduction of IFT and mobilisation of oil.

8.3. Effects of Salinity on IFT

Salinity is largely another major characteristic in defining the IFT between brine and air. The data produced in this study indicates that the IFT decreases with the rise in concentration of NaCl. This is attributable to the impact of salt on the constituent of water molecules. According to [13], sodium chloride ions tend to disturb the hydrogen bonding of water molecules and this type of deterioration in the bonding between water molecules reduces the interfacial tension. The same kinds of results have also been replicated in studies that explored the modifying ability of different salts on IFT in non-aqueous systems of brine and water. It should also be pointed out, though, that the influences on IFT of salinity are not necessarily linear, so that at higher concentrations of salt the IFT can begin to reach a plateau or even rise slightly, depending upon the ions being used. Interactions among salt ions, water molecules, and any surfactants or additives involved are quite complicated, so it is crucial to take them into account to grasp the consequences of salinity on IFT [14].

8.4. Effect of Nanoparticles Polymer-Silica

The inclusion of polymer-silica nanoparticles on the brine-oil system was found

to lower the IFT to a significant level as evidenced in the results emblazoned in Table 4. This behavior has attracted wide attention in nanofluid-enhanced EOR due to the knowledge that nanoparticles adsorb at the oil and water interface, promoting a reduced interfacial tension and enhanced oil displacement [15]. It is probable that the nanoparticles have a role of stabilising that minimises the attraction between the oil and brine phases making separation possible. The decrease in IFT reported in this research matches up with results of other research that have worked with nanoparticle application to decrease IFT in different fluid systems.

The Arabic gum further contributed to the decrease in IFT, presumably because it forms a protective coating at the interface and, thus, this prevents the coalescence of the droplets to keep the system stable [16]. This has been observed before in literature because naturally occurring polymers like Arabic gum have been used in altering the properties of a surfactant system to ensure that they increase the rate of oil recovery.

8.5. Enhanced Oil Recovery (EOR) Implications

This research has extensive implications on enhanced oil recovery (EOR) processes, especially where brine and dead oil are used in a system. The lowering of IFT with an increase in temperature and salinity indicates that EOR processes may be enhanced by temperature and salinity regulation to enhance the reduction in IFT which helps in mobilisation of the trapped oil in reservoirs [17]. The effective induction of nanoparticles and natural polymers also increases the prospects of lowering IFT, thus, presenting an interest in investigating these additives as an opportunity in future research of EOR.

Also, it allows such approaches as utilising brine with different NaCl content and nanoparticle addition as a potential solution to adapting IFT to a particular reservoir scenario to enhance the effectiveness of the recovery process. Still, additional research is needed to find out how stable this kind of system is over time and how well it works in the field.

9. Conclusions

For this investigation, the IFT was determined by using the pendant drop (risen bubble) approach for the air-water, air-brine, and fluids (silica + Arabic gum) system. To this analysis, the temperature range was considered from 25 to 55 degrees Celsius, and the pressure was from 25 to 1900 pounds per square inch. The influence that temperature, fluid (Silica + Arabic gum), and salinity (NaCl) had on the IFT was shown and confirmed by the results of the experiment. Several pieces of evidence suggest that IFT has a substantial impact on the process of mass transfer from air molecules to water molecules.

The addition of sodium chloride (NaCl) resulted in a decrease in the amount of dissolved air in the water. This caused an increase in the interfacial area of the air bubble, consequently leading to an increase in the interfacial tension (IFT) that was observed. Several different temperatures were used in the IFT experiment,

which was conducted to improve oil recovery using gum Arabic polymer and silica nanoparticles. Within the scope of the experiment, nanoparticles produced from brine were used at a range of concentrations, and nanoparticles generated from distilled water were utilised in a range of concentrations that were equivalent to one another. In addition to this, there is a connection between the size of the bubble and the IFT values that are obtained.

Conflicts of Interest

The authors declare no conflicts of interest regarding the publication of this paper.

References

[1] Nikolova, C. and Gutierrez, T. (2020) Use of Microorganisms in the Recovery of Oil from Recalcitrant Oil Reservoirs: Current State of Knowledge, Technological Advances and Future Perspectives. *Frontiers in Microbiology*, **10**, Article ID: 2996. https://doi.org/10.3389/fmicb.2019.02996

[2] Ahmed, S. and Elraies, K.A. (2018) Microemulsion in Enhanced Oil Recovery. In: Karakuş, S., Ed., *Science and Technology Behind Nanoemulsions*, InTech, 145. https://doi.org/10.5772/intechopen.75778

[3] Emmanuel, B.N., Peter, D.A., Peter, M.O., Adedayo, I.S. and Olaifa, K. (2025) Helicobacter Pylori Infection in Africa: Comprehensive Insight into Its Pathogenesis, Management, and Future Perspectives. *Journal of Umm Al-Qura University for Applied Sciences*, **11**, 378-401. https://doi.org/10.1007/s43994-024-00166-6

[4] Sakhadeo, N.N. and Patro, T.U. (2022) Exploring the Multifunctional Applications of Surface-Coated Polymeric Foams—A Review. *Industrial & Engineering Chemistry Research*, **61**, 5366-5387. https://doi.org/10.1021/acs.iecr.1c04945

[5] Yarranton, H.W. and Masliyah, J.H. (1996) Gibbs-Langmuir Model for Interfacial Tension of Nonideal Organic Mixtures over Water. *The Journal of Physical Chemistry*, **100**, 1786-1792. https://doi.org/10.1021/jp952017n

[6] Zhang, Y., Liu, Z.R., Yao, B.N., Legut, D. and Zhang, R.F. (2023) Atomic Insights into Interface-Mediated Plasticity and Engineering Principles for Heterogeneous Serrated Interfaces. *International Journal of Plasticity*, **160**, Article 103498. https://doi.org/10.1016/j.ijplas.2022.103498

[7] Massarweh, O. and Abushaikha, A. (2022) Novel Surfactant Formulations Tailored for Enhanced Oil Recovery Purposes: Physicochemical Properties at Various Salinity Levels. *Fourth EAGE WIPIC Workshop*, **2022**, 1-5. https://doi.org/10.3997/2214-4609.20224103

[8] Zhou, W., Chen, J., Dai, R. and Wang, Z. (2025) Selective Removal of Organic Matters from High-Salinity Chemical Industrial Wastewater: Ultrafiltration or Nanofiltration? *Water Research*, **282**, Article 123762. https://doi.org/10.1016/j.watres.2025.123762

[9] Bagalkot, N. and Hamouda, A.A. (2018) Diffusion Coefficient of Co_2 into Light Hydrocarbons and Interfacial Tension of Carbonated Water-Hydrocarbon System. *Journal of Geophysics and Engineering*, **15**, 2516-2529. https://doi.org/10.1088/1742-2140/aad432

[10] Saad, S.M.I. and Neumann, A.W. (2015) Laplacian Drop Shapes and Effect of Random Perturbations on Accuracy of Surface Tension Measurement for Different Drop Constellations. *Advances in Colloid and Interface Science*, **222**, 622-638.

https://doi.org/10.1016/j.cis.2014.10.008

[11] Farhadi, H., Mahmoodpour, S., Ayatollahi, S. and Fatemi, M. (2023) A Novel Oil/Brine Surface Complexation Model: Capturing the Dynamic Nature of the Interface Using IFT. *Journal of Molecular Liquids*, **391**, Article 123359. https://doi.org/10.1016/j.molliq.2023.123359

[12] Massarweh, O. and Abushaikha, A.S. (2020) The Use of Surfactants in Enhanced Oil Recovery: A Review of Recent Advances. *Energy Reports*, **6**, 3150-3178. https://doi.org/10.1016/j.egyr.2020.11.009

[13] Zhang, C. and Carloni, P. (2012) Salt Effects on Water/Hydrophobic Liquid Interfaces: A Molecular Dynamics Study. *Journal of Physics*: *Condensed Matter*, **24**, Article 124109. https://doi.org/10.1088/0953-8984/24/12/124109

[14] Akhlaghi, N., Riahi, S. and Parvaneh, R. (2021) Interfacial Tension Behavior of a Nonionic Surfactant in Oil/Water System; Salinity, Ph, Temperature, and Ionic Strength Effects. *Journal of Petroleum Science and Engineering*, **198**, Article 108177. https://doi.org/10.1016/j.petrol.2020.108177

[15] Liu, Y., Li, H.A. and Okuno, R. (2016) Measurements and Modeling of Interfacial Tension for CO_2/CH_4/Brine Systems under Reservoir Conditions. *Industrial & Engineering Chemistry Research*, 55, 12358-12375. https://doi.org/10.1021/acs.iecr.6b02446

[16] Yang, Q., Qian, Y., Zhou, H. and Yang, S. (2016) Conceptual Design and Techno-Economic Evaluation of Efficient Oil Shale Refinery Processes Ingratiated with Oil and Gas Products Upgradation. *Energy Conversion and Management*, **126**, 898-908. https://doi.org/10.1016/j.enconman.2016.08.022

[17] Nyah, F., Ridzuan, N., Aziz, M.A.B., Gbonhinbor, J., Money, B., Nwaichi, P.I., *et al.* (2025) Bibliometric Insights into Cellulose Nanoparticles: Advancing Sustainable Enhanced Oil Recovery in HTHP Reservoirs. *SPE Nigeria Annual International Conference and Exhibition*, Lagos, 4-6 August 2025, SPE-228643-MS. https://doi.org/10.2118/228643-ms